Coordination Chemistry Reviews 254 (2010) 1295–1306

Contents lists available at ScienceDirect

Coordination Chemistry Reviews

journal homepage: www.elsevier.com/locate/ccr

Review

Metallophosphoranes: The hidden face of transition metal–phosphine complexes

Jenni Goodman, Stuart A. Macgregor*

School of Engineering & Physical Sciences, Heriot-Watt University, Riccarton, Edinburgh, Lothian EH14 4AS, UK

Contents

ARTICLE INFO

Article history:
Received 14 July 2009
Accepted 4 February 2010
Available online 11 February 2010

Keywords:
Metallophosphoranes
Mechanism
Density functional theory
Isomerization
M–X/P–R exchange
Bond activation
C–F activation
Phosphine ligands

ABSTRACT

Reactions in which metallophosphoranes, of general formula L$_n$MPR$_4$, have been implicated as intermediates or possible transition states are reviewed. Such species can be accessed via nucleophilic attack on metal–phosphine complexes, with the source of nucleophile being either external or internal in the form of an anionic co-ligand. The reverse process, transfer of a group from a {PR$_4$} ligand to a metal, has also been observed with the formation of a metal phosphine. Thus metallophosphoranes have been postulated to play a role in isomerization processes and novel M–X/P–R exchange reactions. Metallophosphoranes have also been implicated in unusual 'phosphine-assisted C–F bond activation' reactions. Recent computational studies on these processes are discussed.

1. Introduction

Metallophosphoranes (L$_n$MPR$_4$) are analogous to the pentavalent phosphoranes (PR$_5$) of main group chemistry, where one substituent is replaced by a metal-based moiety. This review will focus on cases where L$_n$M is a transition metal-based fragment and will consider the reactivity of such systems, in particular those processes that involve interconversion with transition metal–phosphine complexes. Metallophosphoranes are often formulated as complexes of anionic phosphoranide ligands, [PR$_4$]$^-$, with a cationic metal centre, L$_n$M$^+$, implying a formal P(III) oxidation state at the central phosphorus (Scheme 1). The general area of metallophosphorane chemistry has been the subject of a number of previous reviews [1–3].

2. Structural properties

The first crystallographically characterized metallophosphorane, **1**, was reported by Riess and coworkers in 1981 [4] and a search of the Cambridge Structural Database now reveals more than 30 metallophosphoranes, including examples from Group 6 (Mo [5]), Group 7 (Mn [6]), Group 8 (Fe [7], Ru [8]), Group 9 (Co [9], Rh [10], Ir [11]) and Group 10 (Ni [12], Pd [13], Pt [10b,14]). The structures of metallophosphoranes generally fall into two cat-

* Corresponding author. Tel.: +44 0131 451 8031; fax: +44 0131 451 3180.
E-mail address: s.a.macgregor@hw.ac.uk (S.A. Macgregor).

0010-8545/$ – see front matter © 2010 Elsevier B.V. All rights reserved.
doi:10.1016/j.ccr.2010.02.002

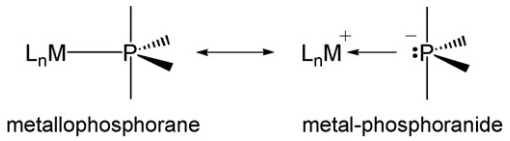

Scheme 1.

egories – a simple κ^1-binding mode through phosphorus (as in **2** [6], **3** [10a] and **4** [11]) and a κ^2-binding mode, where a heteroatom substituent on phosphorus can also donate to the metal centre (as in **1**). In the former case the geometry around phosphorus is usually close to trigonal bipyramidal, whereas the κ^2-species display more distorted structures and are formed when the metal centre would otherwise be unsaturated.

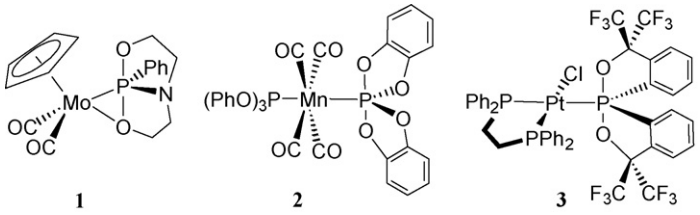

To date all the crystallographically characterized metallophosphoranes feature at least two electronegative substituents at phosphorus and examples of $\{PN_4\}$, $\{PO_4\}$ (e.g. **2**), $\{PN_2O_2\}$ and $\{PO_2C_2\}$ (e.g. **3**) species are particularly prevalent. Substituents at phosphorus are usually cyclic in nature and to date only one metallophosphorane, $[IrCl_2(PF_4)(CO)(PEt_3)_2]$, **4**, has been characterized in the solid state where all four substituents at phosphorus are non-cyclic. Further examples of metallophosphoranes devoid of cyclic groups have been characterized in solution, although it is noticeable that these all feature at least three highly electronegative F [15] or Cl [16] substituents. In cases where the four groups around phosphorus are equivalent the bonds to the axial substituents are always longer than those to the equatorial substituents. Moreover, in κ^2-species one axial substituent can be considered as bridging the metal and phosphorus centres and so elongation of this bond is usually even more pronounced. When there is a choice (as for example in $\{PN_2O_2\}$ and $\{PO_2C_2\}$ species) the most stable isomer features the more electronegative substituents in the axial positions, as in **1** and **3**. These structural patterns are similar to the well-established behaviour of main group phosphoranes and are a result of the delocalized 3c–4e bonding along the axial direction [17]. As the late transition metal fragments in metallophosphoranes are relatively electron rich they always adopt an equatorial position. This site may also be preferred as it allows more favourable MPR_4 π-back donation [7a], as well as providing more space for the more sterically encumbered L_nM moieties.

3. Synthesis and reactivity

The synthesis of metallophosphoranes has been reviewed previously [1–3] and so will only be briefly outlined here. General methods are summarized in Fig. 1 and include (A) intramolecular nucleophilic attack at a bound phosphine, (B) external nucleophilic attack at bound phosphine, (C) addition of halogens to metal-phosphido species, (D) S_N2 displacement of halide from a halophosphorane by an electron-rich organometallic and (E) metathesis of a M-halide bond by a phosphoranide.

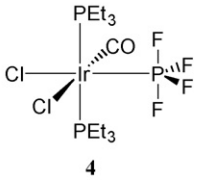

Of particular interest in this review are methods A and B, which highlight the close relationship between metallophosphoranes and transition metal–phosphine complexes. Indeed method A was the basis of the syntheses of several early metallophosphoranes by Riess and coworkers arising from their studies of the coordination chemistry of aminophosphoranes such as **5** (Scheme 2) [4,5a,18]. Reaction of **5** with $[MClCp(CO)_3]$ (M = Mo, W) yields **6** in which the aminophosphorane is present in its NH tautomer and thus binds through the phosphorus centre. Subsequent halide abstraction causes rearrangement to **7** featuring a P,N-bidendate donor ligand. Low temperature deprotonation of **7** with MeLi forms the corresponding amide, **8**, which upon warming to room temperature induces an intramolecular nucleophilic attack to give metallophosphorane **9**. Further heating results in isomerization to the final product **1**. **1** is therefore thermodynamically more stable than **9** and, consistent with this, features both electronegative O substituents in axial positions. **1** and **9** are both κ^2-metallophosphoranes in which either an axial N or O substituent, respectively, bridges the M–P bond.

Riess subsequently exploited this methodology to prepare a range of similar metallophosphoranes with Fe and Ru [18,19] and also extended this chemistry to cyclamphosphorane precursors [5b]. A related synthetic methodology was developed by Nakazawa

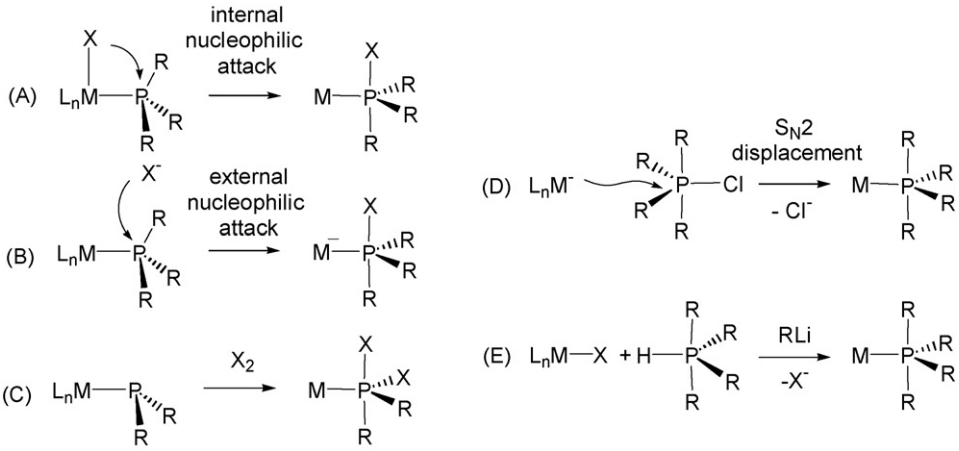

Fig. 1. General methods of preparation of metallophosphoranes. Adapted from Ref. [2].

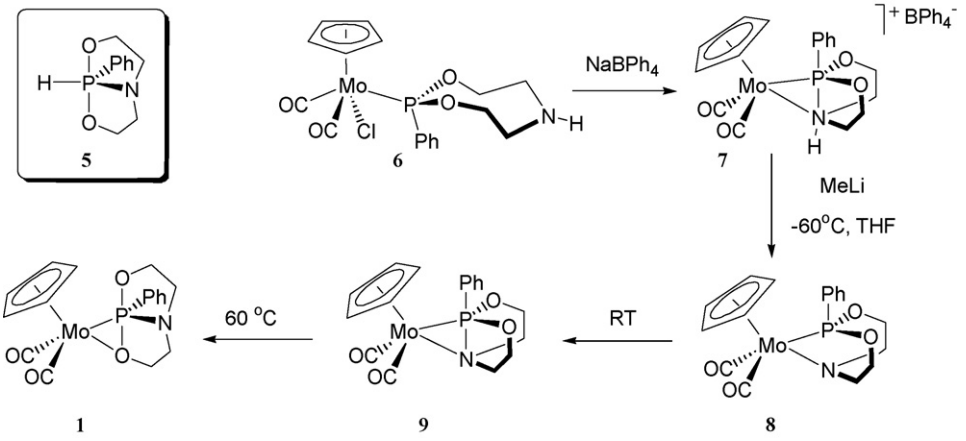

Scheme 2.

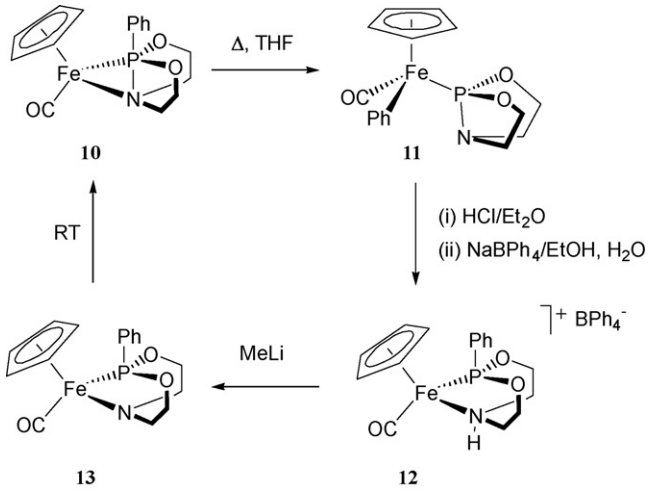

Scheme 3.

and coworkers who showed that displacement of OR^- from phosphite ligands was possible under the action of F^- as an external nucleophile. Thus reaction of $[Fe(Cp)(CO)(L)P(OPh)_3]^+$ with NEt_4F resulted in the formation of $[Fe(Cp)(CO)(L)(PF_4)]$ (L = CO, $P(OPh)_3$) and $[Fe(Cp)(CO)(L)(PF_3OPh)]$ (L = CO) [15b].

Just as metallophosphoranes can be produced from metal–phosphine precursors, so can the reverse process occur. Thus heating the iron metallophosphorane, **10**, in THF results in migration of the phenyl substituent to the iron centre, with displacement of the N substituent of the κ^2-phosphoranide ligand to give **11** (see Scheme 3) [18]. The subsequent reformation of **10** from **11** also proved possible, with treatment with gaseous HCl giving amine **12** in which the phenyl group has again transferred from Fe to P. Deprotonation then gives amide **13** which upon intramolecular nucleophilic attack yields **10**. These processes demonstrate the potential for reversible interconversion between metal–phosphine and metallophosphorane species.

Other examples of group transfer from the phosphorus of a metallophosphorane to a neighbouring metal have been established. Miyamoto reported that heating species **14** resulted in transfer of one of the naphthyl moieties from P to Ir (Scheme 4) [20]. Heating to reflux in ethanol resulted in displacement of Cl^- from the metal (**15**), while heating to higher temperatures in xylene saw the displacement of the PMe_3 co-ligand (**16**). This process suggests that hydrocarbyl groups have a greater migratory aptitude than more electronegative O- or N-based substituents, at least when the direction of the transfer is from phosphorus to a metal. Riess also reported the transfer of the allyl group in **17**, to generate the vinyl species **18** (Eq. (1)). The mechanism in this case is thought to involve an Fe-promoted 1,3-shift of the allylic proton coupled with P–C bond cleavage. Interestingly, vinyl and benzyl analogues of **17** did not exhibit any evidence for hydrocarbyl group transfer [19].

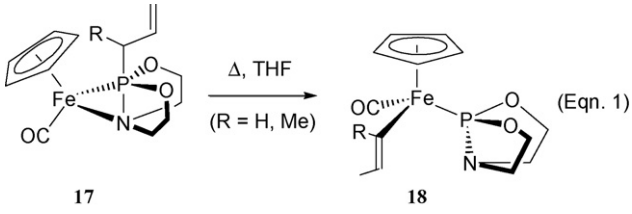

(1)

4. Metallophosphoranes as proposed reaction intermediates

In addition to the above examples where metallophosphoranes have been directly observed, these species have also been postulated as intermediates in a range of different processes. As early as 1971 Green proposed that a metallophosphorane may be implicated in the room temperature reaction of $[NiCl_2(PPh_3)_2]$ with MeMgBr that resulted in Me/Ph exchange and formation of

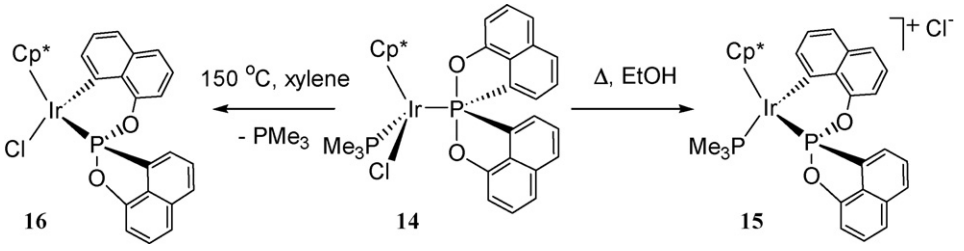

Scheme 4.

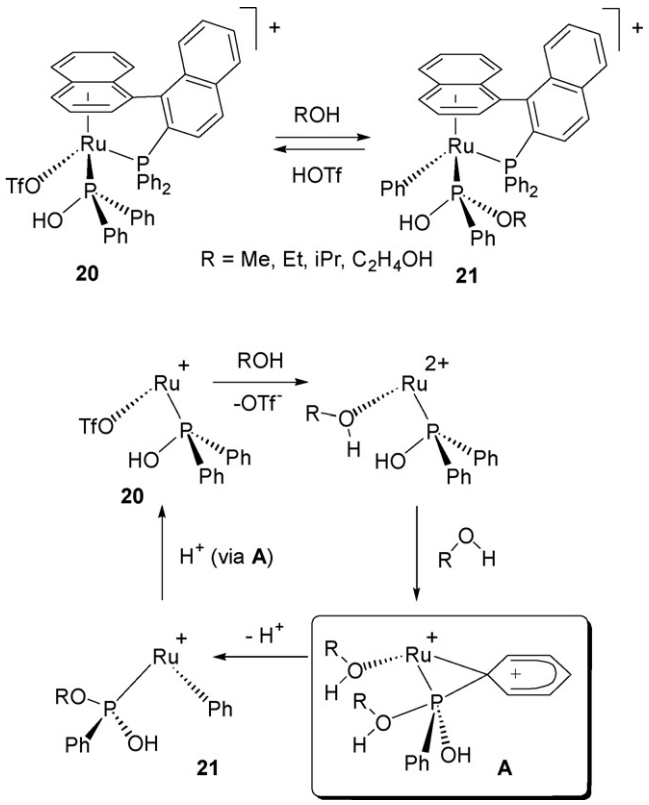

Fig. 2. Interconversion of **20** and **21** and the proposed mechanism involving a metallophosphorane-like species, **A**.

free PMe_2Ph and $PMePh_2$ [21]. Pregosin also suggested that the reversible conversion of **20**–**21**, in which Ph/OR substitution occurs at phosphorus with transfer of Ph onto Ru, may involve an intermediate or transition state, **A**, that resembles a metallophosphorane (see Fig. 2) [22]. In several cases a phosphine has been postulated to be the site of initial nucleophilic attack, although subsequent steps have masked any putative metallophosphorane intermediates. Examples include the reaction of $[FeCp(CO)_2(PHPh_2)]^+$ with $NaBH_4$ to give $[FeCp(H)(CO)_2]$ [23,24] and the decomposition of $[FeCp(CO)_2\{P(NC_4H_8)(OMe)_2\}]^+$ to give $[FeCp(CO)_2\{P(O)(OMe)_2\}]$ in the presence of hydroxide [25].

Metallophosphoranes have also been implicated in disproportionation reactions of Pd(II)–phosphine complexes, a common initiation step in catalysis that produces active Pd(0) species and P(V) byproducts. An early example was the fluoride-induced disproportionation of $[PdCl_2L_2]$ complexes ($L = PPh_3$, $L_2 = Ph_2P(CH_2)_nPPh_2$, $n = 1$–4) to give $[Pd(PPh_3)_4]$ or $[Pd(L_2)_2]$ species and Ph_3PF_2 [26]. The proposed mechanism is shown in Fig. 3 for $L = PPh_3$ and invokes the formation of a metallophosphorane, **22**, via either (i) direct attack at phosphorus or (ii) F^- addition to Pd followed by transfer to phosphorus. Disproportionation occurs in the following step upon loss of the $[PFPh_3]^+$ cation which is trapped by additional F^- to give PF_2Ph_3, while the Pd(0) species formed are trapped by excess phosphine. In the presence of trace water $Ph_3P{=}O$ is the dominant P(V) species that is formed. Mechanistic studies of disproportionation of $[PdCl_2L_2]$ induced by OH^- [27] and acetate [28] have also proposed nucleophilic attack at a bound phosphine as a key step. In the former case studies with chiral phosphines indicate that this process must be intramolecular and involves $[PdCl(OH)(PPh_3)_2]$ as an intermediate. The possibility of such processes involving a metallophosphorane has been discussed [29] and separate calculations suggest that attack of OH^- at a bound PH_3 ligand is certainly energetically accessible [30].

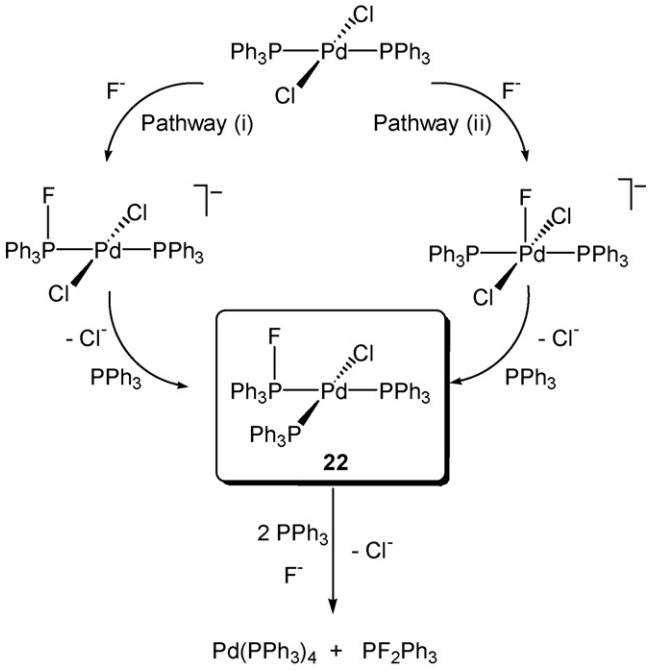

Fig. 3. Proposed mechanism of F^--induced disproportionation of $[PdCl_2(PPh_3)_2]$ via metallophosphorane **22**.

4.1. Computational studies

4.1.1. Isomerization of [Pt(Me)(OMe)(CO)(κ¹-P–P)]

Our interest in the role of metallophosphoranes in organometallic reactivity was sparked by a computational study of the isomerization of $[Pt(Me)(OMe)(CO)(\kappa^1\text{-P–P})]$, **23** (where $P–P = Ph_2PCH_2CH_2PPh_2$) [29]. This was part of a wider study modelling the reaction of CO with [Pt(Me)(OMe)(P–P)], **24**, where migratory insertion occurs exclusively into the Pt–O bond to give the methoxycarbonyl, **25** (Eq. (2)) [31].

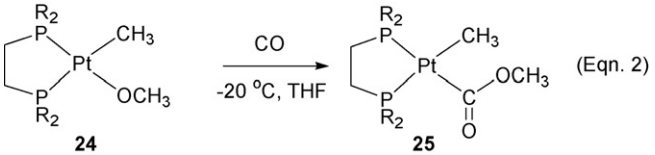

(2)

Density functional theory calculations (R = H, cf. Eq. (2)) showed that the initial coordination of CO readily occurs with displacement of one arm of the bidentate phosphine ligand such that CO is placed *cis* to either Me (**23a**) or OMe (**23b**, see Fig. 4). Although **23a** was the more stable isomer (due to the π-donor OMe being *trans* to CO), insertion into the Pt–OMe bond via **23b** (E(TS) = +12.2 kcal/mol) was calculated to be more accessible than that into the Pt–Me bond of **23a** (E(TS) = +15.2 kcal/mol). The final methoxycarbonyl product, **25**, was also found to be more thermodynamically stable than the alternative acyl, as the C(O)–OMe bond formed in this case is much stronger than an acyl C(O)–Me bond.

At this point the calculations had successfully reproduced the experimental behaviour, with methoxycarbonyl formation being computed to be favoured both kinetically and thermodynamically. A complication arose, however, when a third isomer of the 4-coordinate intermediate, **23c**, was considered. In **23c** CO is *cis* to both the Me and OMe groups and calculations revealed a new low energy pathway for insertion into the Pt–OMe bond (E(TS) = +10.0 kcal/mol). This presented a difficulty, as no direct route to isomer **23c** from the reaction of **24** with CO could be located. Instead it was assumed that isomer **23a** would initially be formed and subsequently undergo isomerization to **23c**.

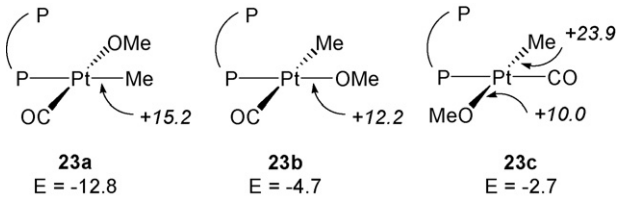

Fig. 4. Geometries and energies (kcal/mol) for the isomers of intermediate **23**. Also indicated in italics are the transition state energies for the various competing CO migratory insertion processes. Energies are relative to the reactants, **24** and CO, set to zero.

In principle, isomerization of a square-planar 4-coordinate species may occur within a 3-coordinate regime (after initial ligand dissociation), a 4-coordinate regime (via a square-planar/tetrahedral/square-planar process) or a 5-coordinate regime (after initial ligand addition). Calculations suggested that the former two processes would be prohibitively high in energy and so the focus fell on the last possibility in which initial coordination of the pendant phosphine arm in **23a** would produce 5-coordinate [Pt(Me)(OMe)(CO)(κ^2-P–P)]. Isomerization in such a d^8 5-coordinate species might be expected to be facile. However, contrary to expectation, the approach of the pendant phosphine arm in **23a** did not lead to a 5-coordinate adduct; instead a new process was characterized in which transfer of the OMe ligand onto the {PH_2} moiety occurred. The transition state for this process, **TS(23a–26)**, shows elongation of the Pt···O distance to 2.34 Å, as well as the approach of the pendant phosphine arm towards both the metal (Pt···P2 = 2.41 Å) and the methoxide oxygen (P2···O = 2.60 Å, see Fig. 5). Characterization of this transition state showed it links to a metallophosphorane intermediate, **26**, in which the phosphoranide ligand is *trans* to CO. Importantly, the barrier to form this metallophosphorane is only 9.2 kcal/mol and so should be readily accessible.

In order to complete the isomerization process transfer of the OMe group from phosphorus back to Pt must occur such that the OMe ligand is placed *trans* to Me as in **23c**. A transition state for this process **TS(26–23c)** was readily located with a structure that complements that of **TS(23a–26)**, with elongation of the Pt···P1 and P2···O distances to 2.57 Å and 2.24 Å, respectively, and a short Pt···O contact of 2.44 Å. In both transition states the OMe ligand is oriented such that its occupied orbitals can effectively bridge the Pt–P vector. In addition, the Pt–CO distances in **26** (1.91 Å) and **23c** (1.88 Å) indicate that the [PH_3(OH)]$^-$ phosphoranide has a higher *trans* influence than the related PH_3 ligand. OMe transfer via **TS(26–23c)** completes the isomerization between **23a** and **23c** which proceeds with an overall barrier of 17.5 kcal/mol and allows the lowest energy CO migratory insertion pathway into the Pt–OMe bond in **23c** to be accessed. More generally, the formation and low energy of intermediate **26** suggested that such novel metallophosphoranes can be readily accessible and could play a wider role in organometallic chemistry than had previously been thought.

4.2. F/Ph exchange in the fluoro congener of Wilkinson's catalyst

In 2004 Grushin and Marshall reported the synthesis and characterization of [$RhF(PPh_3)_3$], **27**, the fluoro congener of Wilkinson's catalyst [32]. **27** displays some remarkable reactivity, in particular the ability to activate the C–Cl bond of chlorobenzene to give *trans*-[$RhCl(PPh_2F)(PPh_3)_2$], **28**, plus biphenyl (Eq. (3)). Overall this process involves C–Cl, Rh–F and P–C bond cleavage, as well as P–F, C–C and Rh–Cl bond formation. This behaviour is in marked contrast to that of [$RhCl(PPh_3)_3$], which under equivalent conditions undergoes PPh_3 dissociation and formation of [$Rh(\mu\text{-}Cl)(PPh_3)_2]_2$.

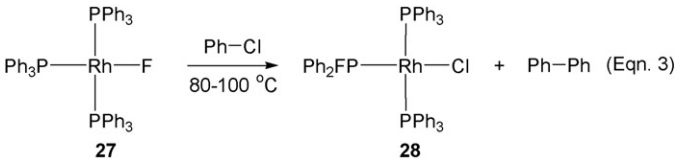

(3)

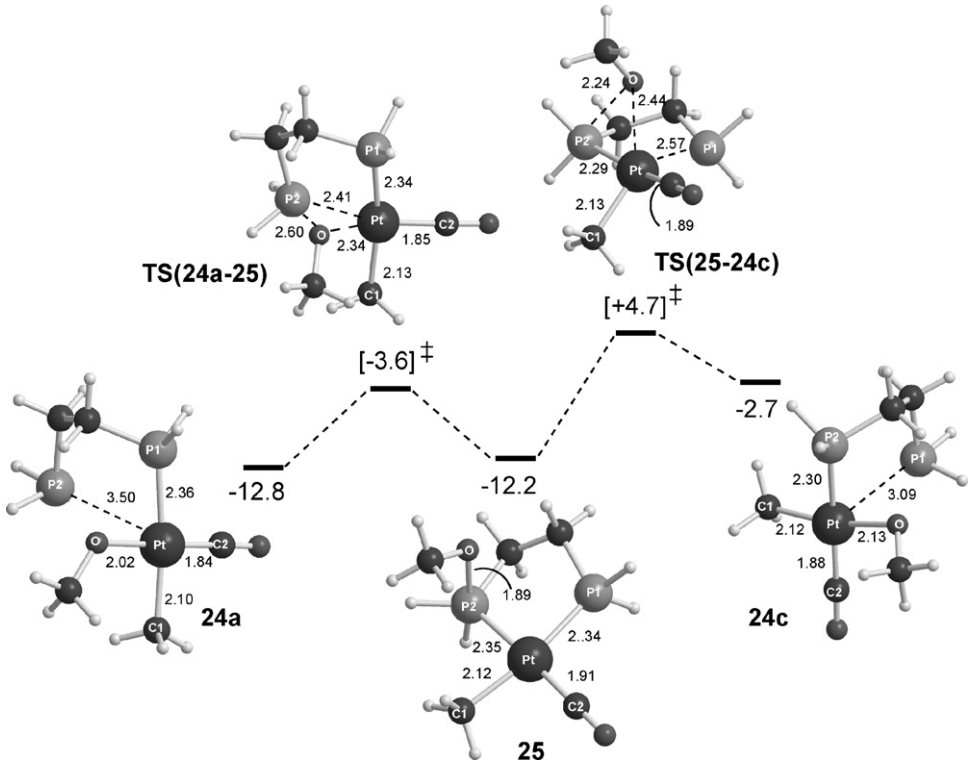

Fig. 5. Computed reaction profile (kcal/mol) for isomerization between **23a** and **23c** via metallophosphorane intermediate **26**. Selected distances are given in Å.

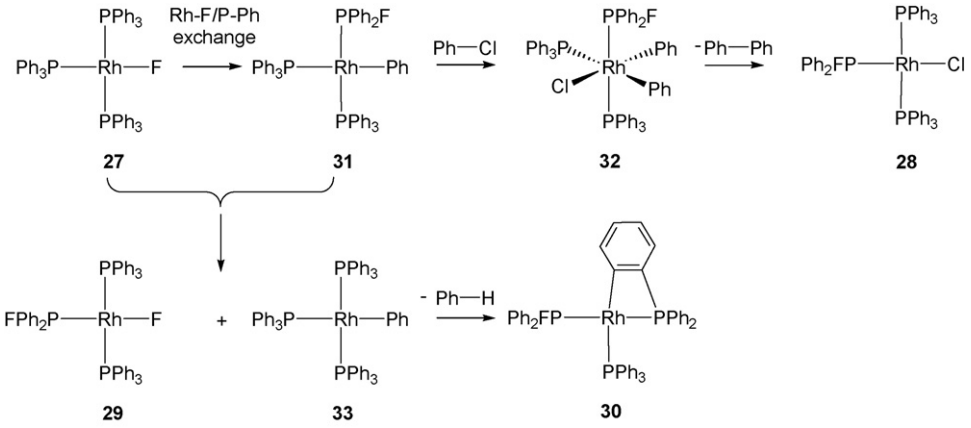

Scheme 5.

Further studies revealed that heating **27** in benzene led to a 1:1 mixture of *trans*-[RhF(PPh_2F)(PPh_3)$_2$], **29**, and the cyclometallated species **30** (Eq. (4)).

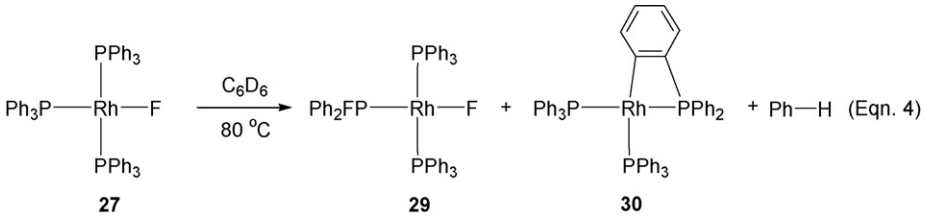

(4)

The key insight that helped rationalize these observations was the possibility of forming [RhPh(PPh_2F)(PPh_3)$_2$], **31**, via Rh–F/P–Ph exchange in **27** (see Scheme 5) [33]. **31** would be sufficiently electron rich to activate chlorobenzene to give **32** which could then form **28** via reductive elimination of biphenyl. Moreover, in benzene **31** can undergo phosphine exchange with **27** to generate **29** and [RhPh(PPh_3)$_3$], **33**, which itself undergoes cyclometallation to **30**. Subsequent experimental studies [34] fully characterized the Rh–F/P–Ph exchange process in **27** and showed that this species is in an approximately 1:1 equilibrium with **31** in benzene at 70 °C. Moreover, activation parameters of $\Delta H^{\ddagger} = 22.0 \pm 1.2$ kcal/mol and $\Delta S^{\ddagger} = -10.0 \pm 3.7$ eu were defined for the Rh–F/P–Ph exchange process.

Despite this detailed experimental characterization of Rh–F/P–Ph exchange in **27** the mechanism by which this transformation occurred was still unknown. We therefore turned to density functional theory calculations to model this process. Importantly, experiment had also shown the rate of exchange was independent of the concentration of added PPh_3, ruling out PPh_3 predissociation as a necessary reaction step. Under this constraint two general routes for Rh–F/P–Ph exchange were proposed (Fig. 6). Along Pathway 1, exchange proceeds by initial Ph group transfer from P to Rh to generate a Rh(III) phosphido intermediate, **34**, from which P–F bond coupling would generate **31**. Alternatively in Pathway 2 initial F transfer from Rh to P gives a metallophosphorane intermediate, **35**, from which Ph group transfer from P to Rh completes the exchange. Ultimately the metallophosphorane route via Pathway 2 was shown to be the more accessible mechanism and so the discussion here will focus on that process.

Initial studies considered a simple model system (R = H, cf. Fig. 6, indicated by a prime in the following) and characterized two variants of Pathway 2, the more accessible of which is shown in Fig. 7. F transfer onto phosphine proceeds via **TS(27–35a)′** with an elongation of the Rh···F distance to 2.40 Å and a shortening of the P1···F distance to 1.90 Å. **TS(27–35a)′** leads to a metallophosphorane structure, **35a′**, in which F occupies an axial position of a distorted trigonal bipyramid centred on P1. Formation of **35a′** also

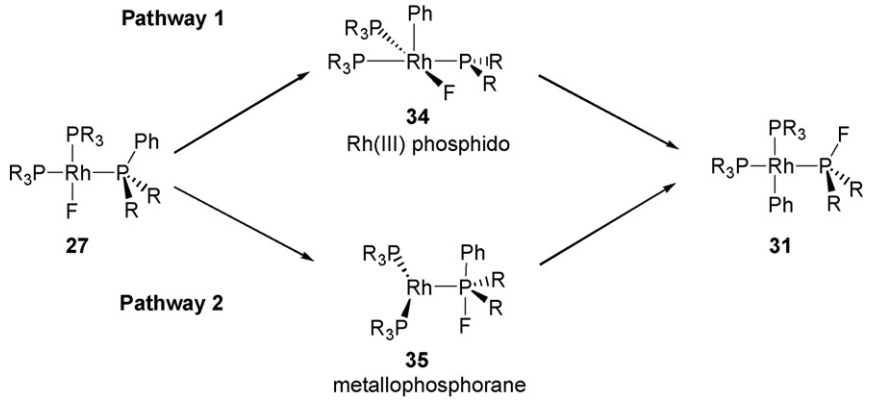

Fig. 6. Proposed mechanisms for Rh–F/P–Ph exchange in **27** (R = Ph).

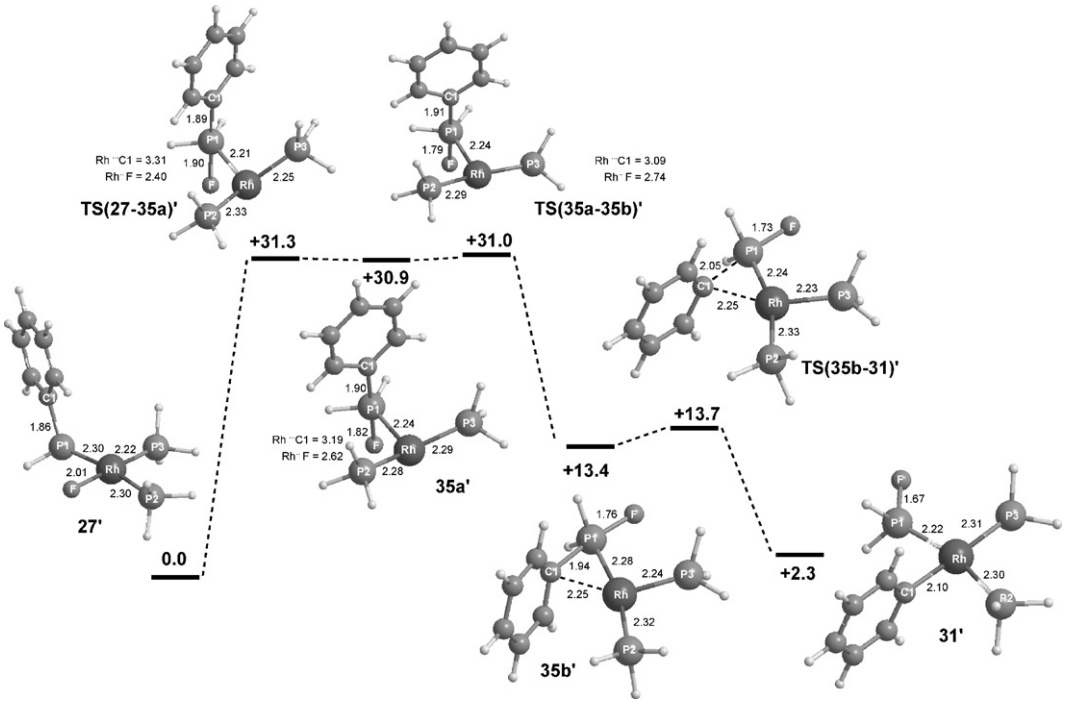

Fig. 7. Computed reaction profile (kcal/mol) for Rh–F/P–Ph exchange in **27**′. Selected distances are given in Å.

involves reorganization of the coordination geometry around Rh such that P2 'follows' the fluoride as it transfers onto P1. This results in the phosphoranide ligand developing *trans* to a vacant coordination site and appears to be driven by the greater *trans* influence of phosphoranides compared to phosphines, as noted above in **26** vs. **23c**.

In order to further the Rh–F/P–Ph exchange process, movement of a *cis* PH_3 ligand in **35a**′ is required to make a *cis* coordination site available for Ph group transfer to Rh. This occurs with a minimal activation barrier via **TS(35a–35b)**′ to give a new intermediate **35b**′. **35b**′ can also be considered as a metallophosphorane, but unlike **35a**′ it exhibits a κ^2-structure in which the axial Ph group stabilizes the Rh centre through interaction with the *ipso*-carbon (Rh···C1 = 2.25 Å). **35b**′ is therefore analogous to the many κ^2-metallophosphoranes characterized experimentally where an axial heteroatom substituent plays this role. The much lower energy of **35b**′ compared to **35a**′ suggests a significant stabilization is gained. Despite this, **35b**′ corresponds to a very shallow minimum and Ph group transfer readily proceeds via **TS(35b–31)**′ to give the final model exchange product, **31**′. The overall barrier for Rh–F/P–Ph exchange in **27**′ is computed to be 31.3 kcal/mol and proceeds via two metallophosphorane intermediates, the formation of one which, **35a**′, is the rate-determining step.

Subsequent calculations characterized one further metallophosphorane structure, **TS(27–35b)**′ (Fig. 8), analogous to **TS(27–35a)**′ but with the phosphoranide moiety *trans* to P2. As a result **TS(27–35b)**′ is significantly higher in energy than either **TS(27–35a)**′ or **35a**′. **TS(27–35b)**′ was shown to link directly to **35b**′ from which Rh–F/P–Ph exchange is completed as in Fig. 7. The higher energy of **TS(27–35b)**′ means this alternative pathway has a higher activation energy of 36.9 kcal/mol and would not be competitive with the route via **35a**′.

Further calculations considered the full experimental system (R = Ph in Fig. 6) and employed hybrid BP86:HF calculations [35]. The reaction profiles computed for the metallophosphorane pathways with this model were similar to those described above, with the key exception that the overall barriers were reduced to 22.3 kcal/mol via **TS(27–35a)** and to 27.5 kcal/mol via **TS(27–35b)**. These lower barriers reflect the greater steric encumbrance of the full model systems and the fact that forming the metallophosphorane-like transition states involves a reduction in coordination number around Rh. Overall Rh–F/P–Ph exchange in **27** is predicted to proceed via a metallophosphorane route via intermediates **35a** and **35b** with an overall barrier of 22.3 kcal/mol, a value in excellent agreement with the experimentally determined value of 22.0 ± 1.2 kcal/mol.

4.3. Phosphine-assisted C–F activation

The unexpected formation of fluorophosphine ligands in **28** and **31** has some parallels in the area of C–F bond activation. For example, Milstein and coworkers reported that the reaction of $[IrMe(PEt_3)_3]$, **36**, with C_6F_6 resulted in the unexpected formation of *trans*-$[Ir(C_6F_5)(PEt_3)_2(PEt_2F)]$, **37**, along with ethene and methane (Eq. (5)) [36]. More recently Perutz and coworkers reported a similar result upon reacting C_5F_5N with $[Pt(PR_3)_2]$ (**38**,

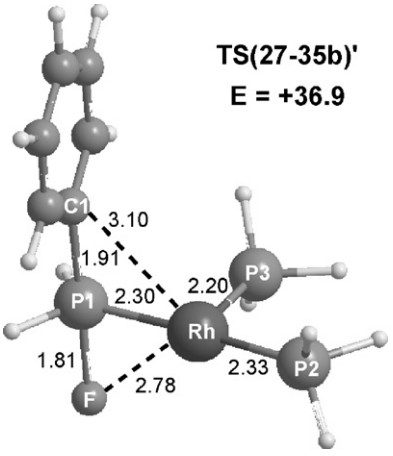

Fig. 8. Alternative initial transition state for Rh–F/P–Ph exchange in **27**′. Selected distances are given in Å.

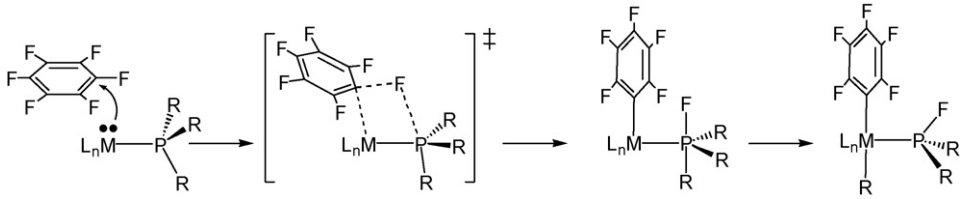

Fig. 9. Proposed mechanism of phosphine-assisted C–F activation.

R = ^{i}Pr, Cy) to give *trans*-[Pt(R)(4-C_5NF_4)(PR_3)(PR_2F)], **39** (Eq. (6)) [37]. Grushin subsequently reported analogous results with C_6F_6 [34].

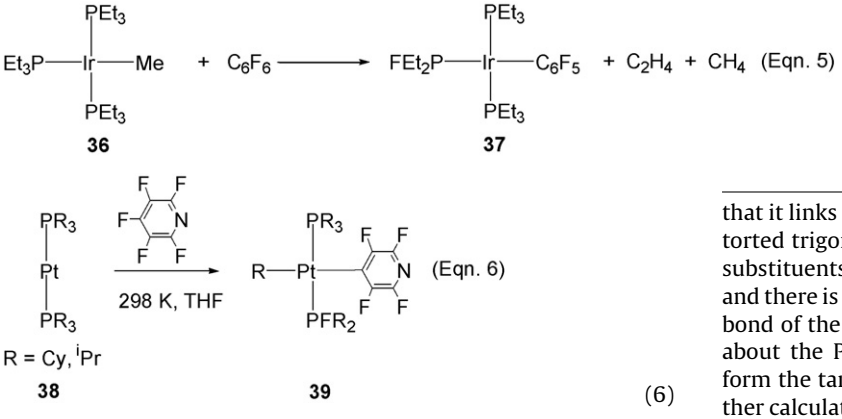

(6)

The feasibility of metallophosphoranes as reactive intermediates led to the suggestion that these species may also be involved in this unusual C–F bond activation chemistry [34]. This proposal is based on the idea that electron-rich metal–phosphine complexes can act as nucleophiles at electron-deficient arenes. Related nucleophilic aromatic substitution reactions have ample precedent in the reactions of transition metal carbonyl anions with perfluorinated arenes, a process that involves displacement of F^- and formation of a new M–aryl bond [38]. This mechanism can be adapted to incorporate a metallophosphorane intermediate if, instead of expelling F^- from the coordination sphere, it is trapped by a neighbouring phosphine ligand (Fig. 9) This concept again exploits the propensity of phosphines to undergo nucleophilic attack, a common feature in metallophosphorane formation, and involves the net addition of a C–F bond over a M–PR_3 bond via a 4-centred transition state. Once the metallophosphorane is formed, transfer of a substituent, R, from phosphorus to the metal centre would produce a fluorophosphine ligand. This sequence could account for the formation of alkyl fluorophosphine species such as **39**, while with **36** would produce an intermediate of the form [Ir(C_6F_5)(Et)(Me)(PEt_3)$_2$(PEt_2F)] from which **37** can be formed via β-H elimination of ethene and reductive elimination of methane.

4.3.1. At [Ir(Me)(PEt_3)$_3$]

Phosphine-assisted C–F activation at [Ir(Me)(PEt_3)$_3$] was initially studied with a simplified *trans*-[Ir(Me)(PH_3)$_2$(PH_2Et)] model system, **36′** [39]. Key computed geometries and energies are shown in Fig. 10 and confirm the anticipated pattern. The two reactants initially form an encounter complex, **40′** with an energy of −5.2 kcal/mol in which the C_6F_6 ring lies approximately parallel to the Ir coordination plane at a distance of about 3.5 Å. Attack of Ir at the *ipso*-carbon leads to a 4-membered transition state, **TS(40–41)′**, featuring incipient Ir···C1 bond formation (2.10 Å) and cleavage of the C1–F1 bond (1.97 Å). The P1···F1 distance is still long at this stage but the {$PEtH_2$} moiety is clearly aligned to accept F1 which, according to a natural charge analysis, is highly nucleophilic in character. Characterization of **TS(40–41)′** confirmed that it links to a metallophosphorane intermediate, **41′**, with a distorted trigonal bipyramidal geometry around P1 and the F and Et substituents in axial positions. Formally, **41′** is an Ir(III) 16e species and there is evidence for a weak agostic stabilization with the β-CH bond of the P–Et group. Disruption of this interaction by rotation about the P–C bond leads to facile Et group transfer onto Ir to form the targeted Ir-ethyl fluorophosphine intermediate **42′**. Further calculations showed that formation of the final model product species **37′** readily occurs via facile β-H elimination of ethene and CH_4 reductive elimination. Phosphine-assisted C–F bond activation therefore occurs with a very reasonable activation barrier of around 19 kcal/mol relative to the precursor adduct **40′**.Alternative routes to the formation of **37′** based on initial C–F bond oxidative addition proved less accessible than this phosphine-assisted mechanism.

In order to probe the factors controlling phosphine-assisted C–F bond activation further calculations were run where the nature of both reactants was varied. A more electron-rich metal centre (*trans*-[Ir(Me)(PMe_3)$_2$(PMe_2Et)]) gave a lower transition state (E = +10.4 kcal/mol), while a more electron-deficient metal centre (*trans*-[IrCl(PH_3)$_2$(PH_2Et)]) caused an increase to +15.6 kcal/mol. These values were shown to correlate with the energy of the metal complex HOMO (predominantly Ir d_z^2 in character) that supplies the electrons for nucleophilic attack. These results suggest that it is the nucleophilicity of the metal centre that controls the accessibility of phosphine-assisted C–F bond activation rather than the Lewis-acidity of the accepting phosphine. This is also reflected in the structures of the transition states involved, which exhibit 'late' geometries in terms of the short forming Ir···C bonds but still have relatively long P···F distances.

The pattern of fluorine substitution around the arene substrate also affects the barrier to phosphine-assisted C–F activation. As shown in Fig. 11 barriers heights are most sensitive to the presence of ortho-F substituents, with each one lowering the barrier by 4–5 kcal/mol (compare **I** vs. **IIIb**, **II** vs. **IVb** and the **IVa/Va/VI** series). A meta-F substituent reduces the barrier by 1–2 kcal/mol (see **I** vs. **IIIa**, **II** vs. **IVa** and the **IVb/Vb/VI** series) whereas a para-F substituent has only a minor effect. These trends are again a reflection of the transition state geometries in which Ir···C bond formation is paramount and are consistent with calculations that indicate that the presence of ortho-F substituents are a key factor in strengthening M–aryl bonds [40].

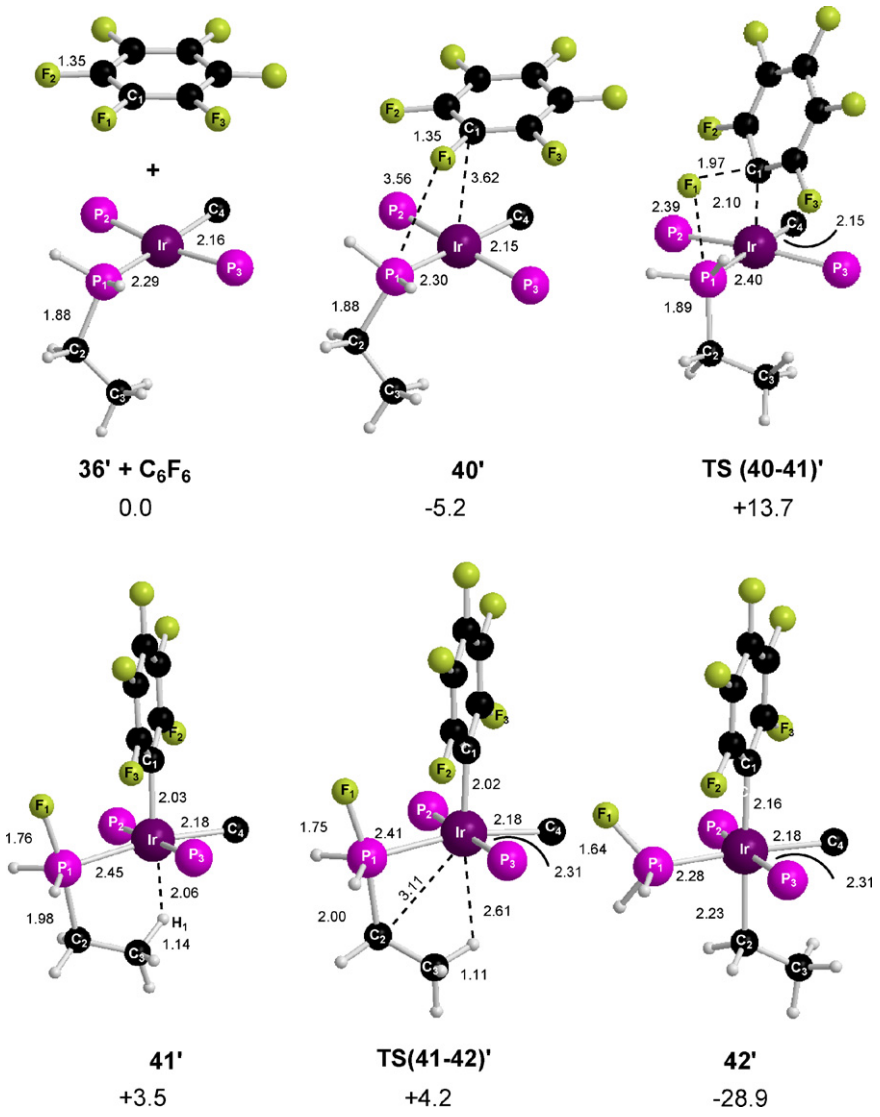

Fig. 10. Computed stationary points for phosphine-assisted C–F activation of C_6F_6 by **36**′ and subsequent Et transfer to form **42**′. Relative energies are in quoted relative to the isolated reactants set to zero and selected distances are given in Å.

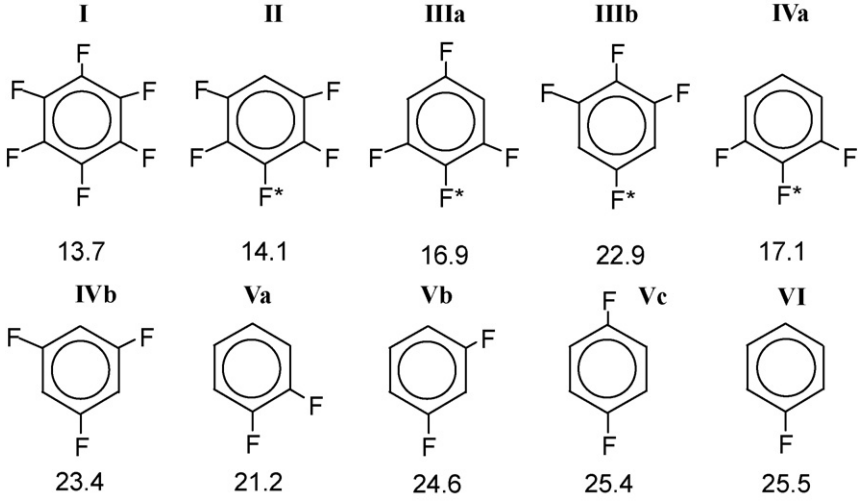

Fig. 11. Computed activation energies (kcal/mol) for phosphine-assisted C–F activation of fluoroarenes by **36**′. Barriers are quoted relative to the isolated reactants set to zero and, where necessary, the activating C–F bond is denoted with an asterisk.

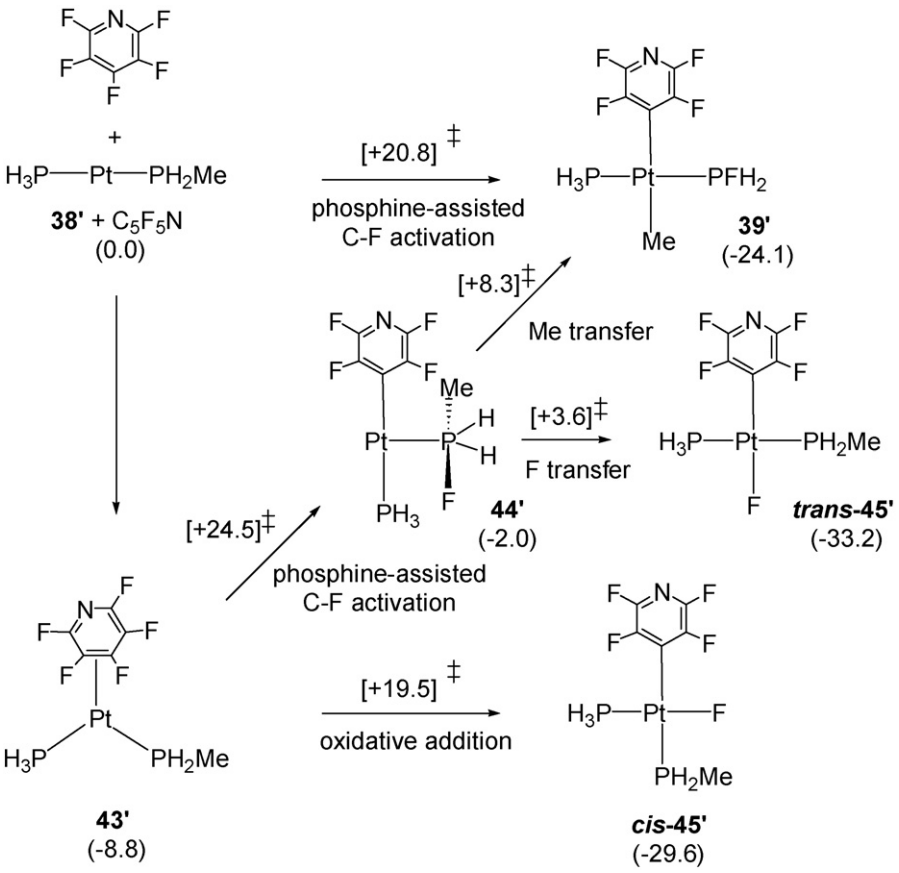

Fig. 12. Computed reaction scheme for C_5F_5N with [$Pt(PH_3)(PH_2Me)$]. Energies (kcal/mol) for minima are given in parenthesis and those for transition states in square brackets.

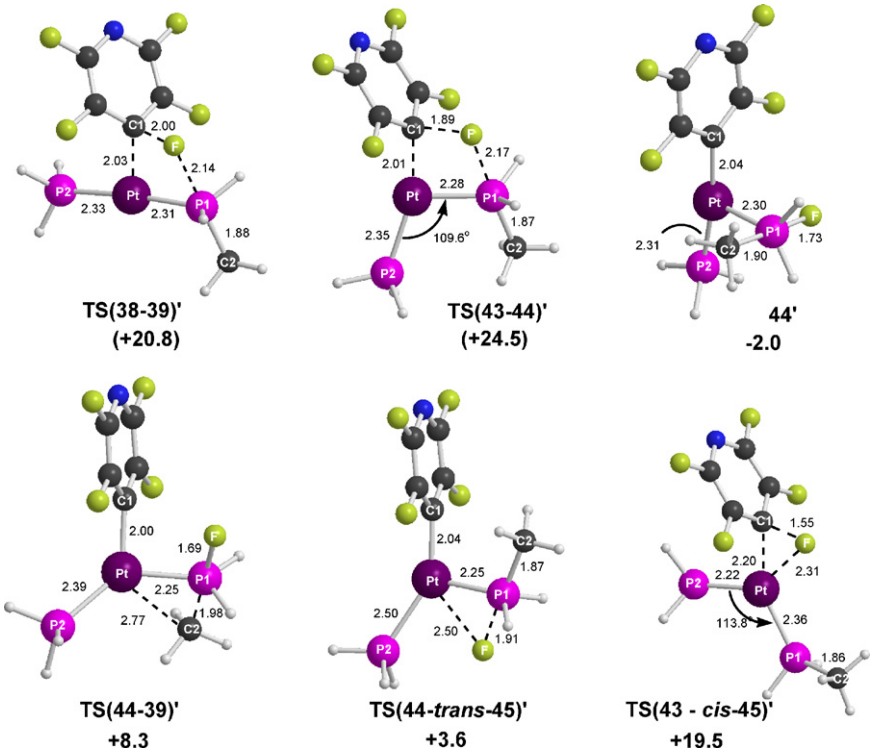

Fig. 13. Computed stationary points arising from C–F Activation of C_5F_5N by [$Pt(PH_3)(PH_2Me)$], **38′**. Energies (relative to isolated reactants) are given in kcal/mol and selected distances in Å.

4.3.2. At [Pt(PR$_3$)$_2$] (R = ^{i}Pr, Cy)

In the light of the above studies the unusual C–F activation reaction of [Pt(PR$_3$)$_2$], **38**, (R = ^{i}Pr, Cy) with pentafluoropyridine to generate *trans*-[Pt(R)(4-C$_5$NF$_4$)(PR$_3$)(PR$_2$F)], **39**, could be rationalized in terms of a similar phosphine-assisted C–F activation/alkyl group transfer sequence of events. Calculations did indeed confirm this possibility, but also showed the reactive landscape associated with this system to be somewhat more complicated [41]. Studies with the model system [Pt(PH$_3$)(PH$_2$Me)], **38′**, revealed four potential pathways that led not only to the expected Pt(alkyl)(fluorophosphine) product (**39′**), but also to the Pt(fluoride)(alkylphosphine) species, **45′**, as either the *cis*- or *trans*-isomers (Fig. 12). These Pt-fluorides are both significantly more stable than **39′**, indicating that the formation of Pt(alkyl)(fluorophosphine) species must be kinetic in origin.

In this case the reactant, **38′**, was found to react either directly with C$_5$F$_5$N or via initial formation of an adduct, [Pt(PH$_3$)(PH$_2$Me)(η^2-C$_5$F$_5$N)], **43′**. In the former case phosphine-assisted C–F activation proceeds via **TS(38-39)′** in which the {P–Pt–P} unit maintains a near-linear geometry (Fig. 13). This results in transfer of a fluorine onto the PH$_2$Me ligand; however, as the resultant phosphoranide moiety develops *cis* to a vacant coordination site, Me group transfer from P to Pt can also occur. **39′** is therefore formed in one step via a concerted C–F/P–C bond activation process. Alternatively, phosphine-assisted C–F activation from trigonal planar **43′** involves **TS(43–44)′** in which the {P–Pt–P} moiety is bent. As a result the phosphoranide develops *trans* to a vacant site, allowing a metallophosphorane, **44′**, to be located as a local minimum. **44′** is similar to metallophosphorane intermediate **35a** located in the study of Rh–F/P–Ph exchange in [RhF(PPh$_3$)$_3$]. Thus transfer of either axial group from P to Pt in **44′** can occur as soon as the P–Pt–P angle increases to allow access to a *cis* coordination site. Transfer of the F substituent is more accessible than that of the alkyl, with **TS(44–*trans*-45)′** being almost 5 kcal/mol more stable than **TS(44–39)′**.

Overall, the lowest energy pathway for formation of **39′** involves phosphine-assisted C–F activation via **TS(38–39)′** with a barrier of 20.8 kcal/mol. **39′** can also be formed via metallophosphorane intermediate **44′**, although the barrier to phosphine-assisted C–F activation from **44′**is somewhat higher in energy (24.5 kcal/mol). Interestingly, F transfer from **44′** is a facile process and yields an Pt–fluoride aryl species that *appears* to be a product of oxidative addition. However, in this case a phosphine ligand has been used to facilitate C–F activation and has acted as a conduit that delivers fluoride to the metal. This process has therefore been called 'phosphine-assisted C–F oxidative addition'. Also shown in Fig. 13 is the conventional 3-centred oxidative addition transition state that originates from **44′** (E = +19.5 kcal/mol). This transition state is in fact marginally the most stable of all those located, suggesting than an oxidative addition reaction channel should be competitive with phosphine-assisted C–F activation. With C$_5$F$_5$N no evidence for oxidative addition was seen experimentally, however, changing the nature of the substrate to 2,3,5-trifluoro,4-(trifluoromethyl)pyridine did results in an oxidative addition product. This latter reaction is a rare example of conventional C–F oxidative addition at Pt(0) and suggests that a delicate balance exists between the oxidative addition and phosphine-assisted C–F activation pathways.

5. Conclusions

This review of metallophosphorane chemistry has highlighted the dual nature of progress in this area. Experimentally, stable metallophosphoranes have been known for almost 30 years and their synthesis and reactivity are reasonably well understood. Such systems are dominated by cases where the phosphoranide ligand bears two or more electronegative substituents and have provided useful precedent in highlighting the relationship between metallophosphoranes and transition metal phosphine complexes. More recently, computational chemistry (in particular) has implicated metallophosphoranes in a number of fundamental processes, including disproportionation, isomerization, M–X/P–R exchange reactions and C–F activation. Such reactions often involve the transfer of an electronegative group onto a trialkyl- or triaryl-phosphine and the ubiquitous status of these ligands in organometallic chemistry makes such metallophosphorane-based reactivity of general importance. However, the isolation of the metallophosphorane intermediate involved in these processes may yet be problematic and this is underlined in computational studies where they appear as very shallow intermediates or transition states. For this reason metallophosphoranes may well remain 'the hidden face of transition metal phosphine complexes'. However, this underlines the power of modern computational methods in their ability to characterize novel reaction intermediates and transition states. Thus the hidden face can be unmasked allowing a range of unusual reactivity patterns to be understood.

Acknowledgements

We thank the EPSRC and Heriot-Watt University for a PhD studentship (JG) and for support through grant number GR/T28539/01.

References

[1] K.B. Dillon, Chem. Rev. 94 (1994) 1441.
[2] H. Nakazawa, K. Kubo, K. Miyoshi, Bull. Chem. Soc. Jpn. 74 (2001) 2255.
[3] C.D. Montgomery, Phosphorus, Sulfur, Silicon 84 (1993) 23.
[4] J. Wachter, B.F. Mentzen, J.G. Riess, Angew. Chem. Int. Ed. Engl. 20 (1981) 284.
[5] (a) F. Jeanneaux, A. Grand, J.G. Riess, J. Am. Chem. Soc. 103 (1981) 4272;
(b) J.M. Dupart, A. Grand, S. Pace, J.G. Riess, J. Am. Chem. Soc. 104 (1982) 2316;
(c) J.M. Dupart, A. Grand, J.G. Riess, J. Am. Chem. Soc. 108 (1986) 1167;
(d) D.V. Khasnis, H.M. Zhang, M. Lattman, Organometallics 11 (1992) 3748.
[6] S.K. Chopra, S.S.C. Chu, P. Demeester, D.E. Geyer, M. Lattman, S.A. Morse, J. Organomet. Chem. 294 (1985) 347.
[7] (a) R. Kubo, H. Nakazawa, T. Mizuta, K. Miyoshi, Organometallics 17 (1998) 3522;
(b) S.K. Chopra, J.C. Martin, Heteroatom. Chem. 2 (1991) 71.
[8] (a) H. Nakazawa, K. Kawamura, T. Ogawa, K. Miyoshi, J. Organomet. Chem. 646 (2002) 204;
(b) H. Nakazawa, K. Kawamura, R. Kubo, K. Miyoshi, Organometallics 18 (1999) 2961.
[9] (a) M. Lattman, S.A. Morse, A.H. Cowley, J.G. Lasch, N.C. Norman, Inorg. Chem. 24 (1985) 1364;
(b) M. Lattman, S.K. Chopra, A.H. Cowley, A.M. Arif, Organometallics 5 (1986) 677;
(c) P. Demeester, M. Lattman, S.S.C. Chu, Acta Crystallogr. C 43 (1987) 162.
[10] (a) K. Toyota, Y. Yamamoto, K.Y. Akiba, J. Organomet. Chem. 586 (1999) 171;
(b) E.G. Burns, S.S.C. Chu, P. Demeester, M. Lattman, Organometallics 5 (1986) 2383;
(c) K. Kajiyama, T.K. Miyamoto, K. Sawano, Inorg. Chem. 45 (2006) 502.
[11] A.J. Blake, R.W. Cockman, E.A.V. Ebsworth, S.G.D. Henderson, J.H. Holloway, N.J. Pilkington, D.W.H. Rankin, Phosphorus, Sulfur, Silicon 30 (1987) 143.
[12] R. Faw, C.D. Montgomery, S.J. Rettig, B. Shurmer, Inorg. Chem. 37 (1998) 4136.
[13] (a) K. Toyota, Y. Yamamoto, K. Akiba, J. Chem. Res. S (1999) 386;
(b) K. Kajiyama, Y. Hirai, T. Otsuka, H. Yuge, T.K. Miyamoto, Chem. Lett. (2000) 784.
[14] (a) M. Lattman, E.G. Burns, S.K. Chopra, A.H. Cowley, A.M. Arif, Inorg. Chem. 26 (1987) 1926;
(b) D.V. Khasnis, M. Lattman, U. Siriwardane, Inorg. Chem. 28 (1989) 681;
(c) D.V. Khasnis, M. Lattman, U. Siriwardane, Inorg. Chem. 28 (1989) 2594;
(d) U. Siriwardane, D.V. Khasnis, M. Lattman, Acta Crystallogr. C 45 (1989) 1628;
(e) I.S. Mikhel, O.G. Bondarev, V.N. Tsarev, G.V. Grintselev-Knyazev, K.A. Lyssenko, V.A. Davankov, K.N. Gavrilov, Organometallics 22 (2003) 925;
(f) D.V. Khasnis, M. Lattman, U. Siriwardane, H.M. Zhang, Organometallics 11 (1992) 2074.
[15] (a) E.A.V. Ebsworth, J.H. Holloway, N.J. Pilkington, D.W.H. Rankin, Angew. Chem. Int. Ed. Engl. 23 (1984) 630;
(b) K. Kubo, K. Bansho, H. Nakazawa, K. Miyoshi, Organometallics 18 (1999) 4311.
[16] E.A.V. Ebsworth, N.T. McManus, N.J. Pilkington, D.W.H. Rankin, J. Chem. Soc., Chem. Commun. (1983) 484.

[17] (a) R. Hoffmann, J.M. Howell, E.L. Muetterties, J. Am. Chem. Soc. 94 (1972) 3047;
(b) R.J. Hach, R.E. Rundle, J. Am. Chem. Soc. 73 (1951) 4321.
[18] (a) P. Vierling, J.G. Riess, A. Grand, J. Am. Chem. Soc. 103 (1981) 2466;
(b) P. Vierling, J.G. Riess, A. Grand, Inorg. Chem. 25 (1986) 4144.
[19] (a) P. Vierling, J.G. Riess, J. Am. Chem. Soc. 106 (1984) 2432;
(b) P. Vierling, J.G. Riess, Organometallics 5 (1986) 2543.
[20] K. Kajiyama, A. Nakamoto, S. Miyazawa, T.K. Miyamoto, Chem. Lett. 32 (2003) 332.
[21] M.L.H. Green, M.J. Smith, H. Felkin, G. Swierczewski, J. Chem. Soc. D (1971) 158b.
[22] T.J. Geldbach, P.S. Pregosin, Eur. J. Inorg. Chem. (2002) 1907, and references therein.
[23] H. Nakazawa, K. Kubo, C. Kai, K. Miyoshi, J. Organomet. Chem. 439 (1992) C42.
[24] Later density functional theory calculations located the postulated metallophosphorane intermediate but did suggest that hydride attack at CO might be energetically more favourable: D.A. Brown, J.P. Deignan, N.J. Fitzpatrick, G.M. Fitzpatrick, W.K. Glass, Organometallics 20 (2001) 1636.
[25] H. Nakazawa, K. Kubo, K. Tanisaki, K. Kawamura, K. Miyoshi, Inorg. Chim. Acta 222 (1994) 123.
[26] (a) M.R. Mason, J.G. Verkade, Organometallics 9 (1990) 864;
(b) M.R. Mason, J.G. Verkade, Organometallics 11 (1992) 2212.
[27] V.V. Grushin, H. Alper, Organometallics 12 (1993) 1890.
[28] C. Amatore, A. Jutland, Acc. Chem. Res. 33 (2000) 314, and references therein.
[29] S.A. Macgregor, G.W. Neave, Organometallics 23 (2004) 891.
[30] A.A.C. Braga, N.H. Morgon, G. Ujaque, F. Maseras, J. Am. Chem. Soc. 127 (2005) 9298.
[31] H.E. Bryndza, Organometallics 4 (1985) 1686.
[32] V.V. Grushin, W.J. Marshall, J. Am. Chem. Soc. 126 (2004) 3068.
[33] M–X/P–R exchange reactions have been reviewed, see: S.A. Macgregor, Chem. Soc. Rev. 36 (2007) 67.
[34] S.A. Macgregor, D.C. Roe, W.J. Marshall, K.M. Bloch, V.I. Bakhmutov, V.V. Grushin, J. Am. Chem. Soc. 127 (2005) 15304.
[35] S.A. Macgregor, T. Wondimagegn, Organometallics 26 (2007) 1143.
[36] O. Blum, F. Frolow, D. Milstein, J. Chem. Soc. Chem. Commun. (1991) 258.
[37] N.A. Jasim, R.N. Perutz, A.C. Whitwood, T. Braun, J. Izundu, B. Neumann, S. Rothfeld, H.G. Stammler, Organometallics 23 (2004) 6140.
[38] (a) T. Braun, R.N. Perutz, Transition-metal mediated C–F bond activation, in: R.H. Crabtree, D.M.P. Mingos (Eds.), Comprehensive Organometallic Chemistry III, Vol. 1, Elsevier, Amsterdam, 2006, Chapter 26;
(b) R.B. King, M.B. Bisnette, J. Organomet. Chem. 2 (1964) 38.
[39] S. Erhardt, S.A. Macgregor, J. Am. Chem. Soc. 130 (2008) 15490.
[40] (a) E. Clot, C. Megret, O. Eisenstein, R.N. Perutz, J. Am. Chem. Soc. 131 (2009) 7817;
(b) E. Clot, M. Besora, F. Maseras, C. Megret, O. Eisenstein, B. Oelckers, R.N. Perutz, Chem. Commun. (2003) 490.
[41] A. Nova, S. Erhardt, N.A. Jasim, R.N. Perutz, S.A. Macgregor, J.E. McGrady, A.C. Whitwood, J. Am. Chem. Soc. 130 (2008) 15499.